

PACS numbers: 81.15.–z; 52.38.Mf; 79.20.Ds
DOI: 10.1070/QE2014v044n06ABEH015426

Mechanisms of formation of sub- and micrometre-scale holes in thin metal films by single nano- and femtosecond laser pulses

P.A. Danilov, D.A. Zayarnyi, A.A. Ionin, S.I. Kudryashov, S.V. Makarov, A.A. Rudenko, V.I. Yurovskikh, Yu.N. Kulchin, O.B. Vitrik, A.A. Kuchmizhak, E.A. Drozdova, S.B. Odinokov

Abstract. **Mechanisms of formation of sub- and micrometre-scale holes in thin silver and chromium films of variable thickness by tightly-focused single nanosecond IR laser pulses with fluences in the range of $10-10^4$ J cm^{-2} are studied by means of optical and scanning electron microscopy. At the minimal fluences above 5 J cm^{-2}, the micrometre (2–5 μm in radius) holes are produced in these films, accompanying the lateral heat conduction in the film during the pump laser pulse, cavitation at the metallic/glass interface and subsequent explosive removal of the molten film. At the fluences of ~1–10 kJ cm^{-2} much larger (20–40 μm in radius) holes are formed in the film as a result of its heating by the erosive surface microplasma through the lateral heat conduction in the film during the plasma lifetime of the order of a few microseconds. Finally, at the maximal fluences (well above 10 kJ cm^{-2}), the submillimetre holes were produced in these films by intense shock waves, generated in the erosive microplasmas. The comparative analysis of the formation mechanisms for sub- and micrometre-scale holes in the same thin metal films by the single nano- and femtosecond laser pulses is provided.**

Keywords: *nano- and femtosecond laser pulses, thin metal films, sub- and micrometre holes, lateral heat conduction, vaporisation, erosive (ablative) plasma, shock wave.*

1. Introduction

Nanoholes in thin metal films are among the most simple and widely spread elements of nano-optics because the nano-scale propagation, frequency conversion and local enhancement of electromagnetic fields of the optical range in the aperture of the nanoholes are of great interest [1–3]. Similar submicron-size structures, such as hollow nanobumps [4, 5], nanotips [6, 7], and spherical nanoparticles [8–10], formed on the metal film surface under focused laser radiation, also possess unique optical, nonlinear-optical and spectroscopic properties, and are currently actively used in biosensorics, optofluidics, and nanophotonics [11–13]. It is noteworthy that these micron-sized structures are of interest for plasmonics of the mid- and far-IR regions, for example for the surface-enhanced absorption of IR radiation or its reflection [14].

For laboratory spectral research, quite urgent is the formation of large arrays of nanoholes, nanospikes, and nanoedges with millions of nanoelements within the region of sub-millimetre size, which turns out possible as a result of a single exposure of pulsed laser radiation of nano-, pico- or femtosecond duration with different focusing geometry [15–21]. Herewith, the direct (without auxiliary elements of the near-field optics – the needles of the atomic-force microscope or surface films of nanoparticles [22]) impact of tightly focused laser pulses has the best technological prospects which is connected with its versatility and the noncontact nature of the impact, as well as with the possibility of application of this direct laser writing technique in conjunction with the non-laser surface structuring methods.

To date, the dependences of the main parameters of the nano- and microholes (diameter, depth) on the focusing conditions, wavelength, energy and duration of laser radiation pulses [15–21] are systematically studied, wherein the minimal diameters of the holes (up to 30 nm) have been obtained for a nanosecond laser pulse [20], while the sub-micron holes arise under the action of the ultrashort (femto- and picosecond and short sub-picosecond) laser pulses [15–19]. Moreover, an unusual tendency to reducing the size of nanoelements with the increase in the laser pulse duration from tens of femtoseconds to a few picoseconds has been traced [5]. All these facts are contrary to the popular belief that the ultrashort pulses, due to their duration, provide the highest spatial resolution in creating the nanostructured materials, regardless of temporal and spatial scales of the processes of energy and mass transfer that determine the formation of these nanostructures [23]. Herewith, the essence of the problem is that, despite the diversity and large number of actual material [15–21], the formation mechanisms of nano- and microholes in thin films under the action of short and ultrashort laser pulses, which are of great interest for understanding the physics of the nano-scale interaction of laser radiation with matter and for a wide range of applications in laser nano- and microtechnology, remain virtually unexplored.

In particular, in the variety of works dedicated to this subject, a speculation is put forward that the use of ultrashort

P.A. Danilov, S.I. Kudryashov, V.I. Yurovskikh P.N. Lebedev Physics Institute, Russian Academy of Sciences, Leninsky prosp. 53, 119991 Moscow, Russia; National Research Nuclear University 'Moscow Engineering Physics Institute', Kashirskoe sh. 31, 115409 Moscow, Russia; e-mail: sikudr@sci.lebedev.ru;
D.A. Zayarnyi, A.A. Ionin, S.V. Makarov, A.A. Rudenko P.N. Lebedev Physics Institute, Russian Academy of Sciences, Leninsky prosp. 53, 119991 Moscow, Russia;
Yu.N. Kulchin, O.B. Vitrik Institute of Automation and Control Processes, Far Eastern Branch, Russian Academy of Sciences, ul. Radio 5, 690041 Vladivostok, Russia; Far Eastern Federal University, ul. Sukhanova 8, 690091 Vladivostok, Russia;
A.A. Kuchmizhak Institute of Automation and Control Processes, Far Eastern Branch, Russian Academy of Sciences, ul. Radio 5, 690041 Vladivostok, Russia; e-mail: alex.iacp.dvo@mail.ru;
E.A. Drozdova, S.B. Odinokov N.E. Bauman Moscow State Technical University, 2-ya Baumanskaya ul. 5, Bld. 1, 105005 Moscow, Russia

Received 3 March 2014; revision received 20 March 2014
Kvantovaya Elektronika **44** (6) 540–546 (2014)
Translated by M.A. Monastyrskiy

(mainly femtosecond) laser pulses is preferable in the formation of nanoholes and similar nanostructures [3–5, 24, 25]. In this case, the assumed mechanisms of the contact modification between the film and substrate are the removal of the film in the solid or liquid state due to the thermoelastic stresses [26–28], cavitation in the melt [28] and the hydrodynamic expansion and fragmentation of the supercritical fluid of the film material [28], which can define different types of the nano-scale topology of the surface nanostructures. However, the compliance of topology of the surface nanostructures with the mechanisms of their generation under the action of ultrashort laser pulses has not been experimentally established until now.

However, as mentioned above, the authors of [6, 7] demonstrated that some of the nanostructures (nanotips, nanoholes), formed on the surface of gold films with femtosecond laser pulses [3, 25], can be reproduced by employing a cheaper and simple-to-use nanosecond laser source. Therefore, the physical mechanisms of formation of the surface nano- and microstructures by nanosecond laser pulses represent a great interest. As is known, in this case the laser modification may occur as a result of the film removal in the solid or liquid state due to the thermoelastic strains generated therein [29], surface cavitation of one of the adjacent materials at the film–substrate interface with 'blowing off' of a solid or liquid film [5], the hydrodynamic instability of the film melt [30] (including its spinodal decomposition [31]), and, finally, its complete evaporation. The appropriate mechanisms of nanosecond laser modification of thin films have been established for modifying the multi-microscales areas, while their manifestation on the nanometer or (sub) micron scales may be different (the size effect), and this remains to be investigated.

In this paper we report the formation of submicron and microscale holes of varying thickness in thin films of silver and chromium under the action of single tightly focused nanosecond IR laser pulses and femtosecond laser pulses of visible range. The dependence of the sizes of holes on the pulse energy and the topology of modification of the films in the region of the holes have been studied by means of electron and optical microscopy.

2. Experimental

In our experiments, we used a pulsed single-mode Nd:YAG laser RL30Q (SPC 'ELS-94') with a pulse width at half-maximum $\tau_{las} \approx 75$ ns and maximal pulse energy $E_{max} \approx 1.6$ mJ at the stability of ~3%, operating in the regime of fundamental harmonic generation ($\lambda_{las} \approx 1064$ nm). Focusing of laser pulses on the surface of a thin metal film located on a computer-controlled three-axis motorised translational table was carried out at normal incidence using a coated aspherical lens with the numerical aperture NA = 0.5 (C-240TME-B, Thorlabs). The radius of the focal spot w_{opt} at the 1/e level was calculated in the absence of spherical and chromatic aberrations, in accordance with the expression for a Gaussian beam in the air,

$$w_{opt} = \frac{\lambda_{las}\sqrt{n_0^2 - NA^2}}{\pi\sqrt{2}\,NA}$$

(refractive index $n_0 \approx 1$) and amounted to ~0.45 μm.

Similarly, femtosecond laser irradiation of fresh surface areas of the films was carried out using single second harmonic pulses of the Satsuma fibre laser (Amplitude Systemes) with an active medium on Yb ions (wavelength, $\lambda_{las} \approx 515$ nm; spectral width at half maximum, 1.7 nm; pulse duration, $\tau_{las} \approx 0.2$ ps; repetition rate, 0–2 MHz). The pulse energy E in the TEM_{00} mode ($M^2 \approx 1.05$) was smoothly changed in the range of 0.005–5 μJ with the use of the in-built output acousto-optic modulator. Focusing of the ultrashort pulses was carried out at the normal incidence to the surface of the film by means of the same coated aspherical lens at full filling of its aperture. The estimated radius of the focal spot at the 1/e level constituted about 0.2 μm.

The optical-quality silver films (thickness $h \approx 30$, 60 and 80 nm) and chromium films ($h \approx 40$ nm) were used as the test samples, deposited without an underlayer on the surface of the silicate glass slide by means of magnetron sputtering with the grain size of 10 nm. Nano- and microholes were formed in the film by the action of a single laser pulse with a varied energy E. The radii R of the holes on the film surface and their topology were investigated with the JEOL JSM 7001 scanning electron microscope and Altami MET-5 metallographic optical microscope.

3. Formation of microholes by nanosecond laser radiation

3.1. Experimental data

The dependences of the radius R of the holes, made on the surface of the silver films of different thickness, on the laser pulse energy E demonstrate a large scatter (from 2 to 300 μm) of the hole sizes (Figs 1, 2). These dependences are not monotonic, dividing into three characteristic regions of logarithmic growth of R with energy having different slopes $w^2_{dep\,I-III}$ in the coordinates R^2, $\ln(E/E_0)$ ($E_0 = 1$ μJ), corresponding to the three regimes of the laser irradiation (regimes I–III). Qualitatively, these regimes are characterised not only by the appearance of the erosive laser plasma in the second regime and a sharp sound signal of the air shock wave in the third regime, but also by different topology of the edges of the hole and its periphery (Fig. 3). In the first regime, the holes of a small radius (up to 5 μm) have melted edges and traces of spraying of the molten layer (Fig. 3a). The typical radii $w_{dep\,I}$

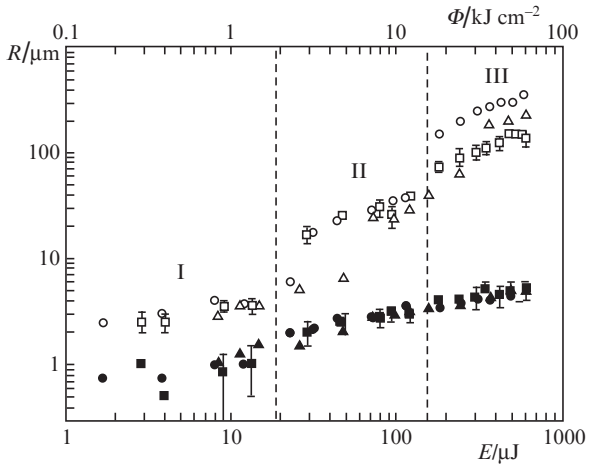

Figure 1. Dependences of the radius R of holes (empty dots) and craters (filled dots) in silver films with the thickness of 30 (□, ■), 60 (○, ●) and 80 nm (△, ▲) on the energy E and the fluence Φ of nanosecond laser pulses for the three regimes of laser action (I–III).

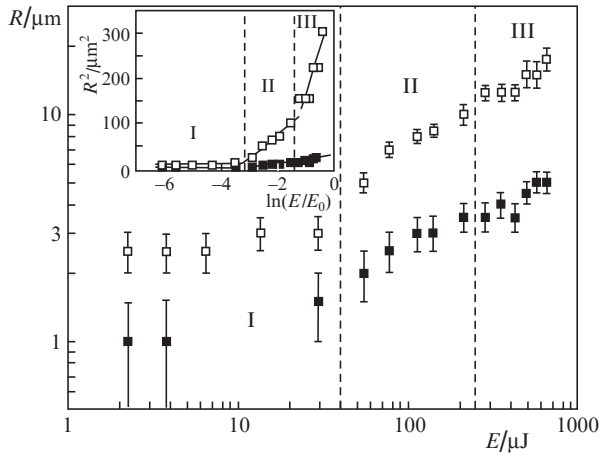

Figure 2. Dependences of the radius R of holes (□) in the chromium film and craters (■) in the glass substrate on the energy E of nanosecond laser pulses for the three regimes of laser action (I–III). The inset shows the same dependences in the coordinates R^2, $\ln(E/E_0)$.

of the holes increase from 2 to 4 μm with increasing silver film thickness h_{Ag}; however, they turn out significantly (approximately twice) less than that those for the chromium film of comparable thickness (Table 1). The topology of the holes and their periphery for the second regime is similar (Fig. 3b) despite the larger size of the holes (10–20 μm, see Fig. 1) and the correspondingly larger slopes $w^2_{dep\,II}$, which increase monotonically with increasing silver film thickness h_{Ag}. For the chromium film of comparable thickness, the characteristic radius is again less (almost three to four times) (Table 1). In contrast, in the third regime, the abnormally large holes with a radius of 200–300 μm ($w_{dep\,III} \sim 100$–300 μm), increasing with h_{Ag}, are formed as a result of the 'cold' removal of the silver films, so that the edges of the removal region are wrapped without melting (Fig. 3c), and the removal itself is of nonuniform nature (Fig. 3d). For the chromium films in this regime, the topology of the ablation region is similar; however, the corresponding characteristic radius is almost an order of magnitude less ($w_{dep\,III} \approx 16$ μm) as a result of a stronger adhesion of the chromium film to the substrate.

Table 1. Measured characteristic radii w (in μm) and threshold energies (given in brackets in μJ) during the formation of the holes and craters in metal films of different thickness in regimes I–III.

Regime	Silver			Chromium
	h = 30 nm	h = 60 nm	h = 80 nm	h = 40 nm
I (hole)	2.5 (1.4)	2.0 (0.33)	4.0 (5.6)	1.2 (0.027)
II (hole)	25 (18)	29 (22)	34 (47)	7.3 (33)
III (hole)	117 (121)	284 (142)	224 (210)	16 (199)
I (crater)	0.76 (2.8)	0.5 (0.24)	1.2 (3.7)	0.7 (0.016)
II (crater)	1.9 (9.6)	2.1 (9.3)	2.3 (18)	2.3 (20)
III (crater)	3.1 (41)	3.4 (69)	3.5 (77)	3.5 (100)

Note: The average error of the radius measurement is about 5%, and that of the threshold energy is up to 25%.

3.2. Interpretation

An important clue to the nature of the regimes of microhole formation arises from the energy dependences of the crater radius R_{crat} on the glass substrate inside these microholes (Figs 1–3), in which these regimes also manifest themselves, albeit to a lesser extent. We should recall that similar craters on the glass substrate in the film holes have been previously observed upon irradiation by single ultrashort (femtosecond) laser pulses and, as follows from these studies, apparently have been wrongly associated with ablation of glass by higher harmonics of the strong laser field generated in the ablation plasma [19]. Meanwhile, in the coordinates R^2_{crat}, $\ln(E/E_0)$ these dependences, for almost all of the films, have the slopes in their initial parts, which correspond to the characteristic radius of the craters $w_{crat\,I} \approx 0.5$–0.7 μm (Table 1) which, within the experimental error in view of the focusing inaccuracies, meets the expected values of the focal spot radius $w_{opt}(1064\text{ nm}) \approx 0.45$ μm for NA = 0.5. This fact indicates

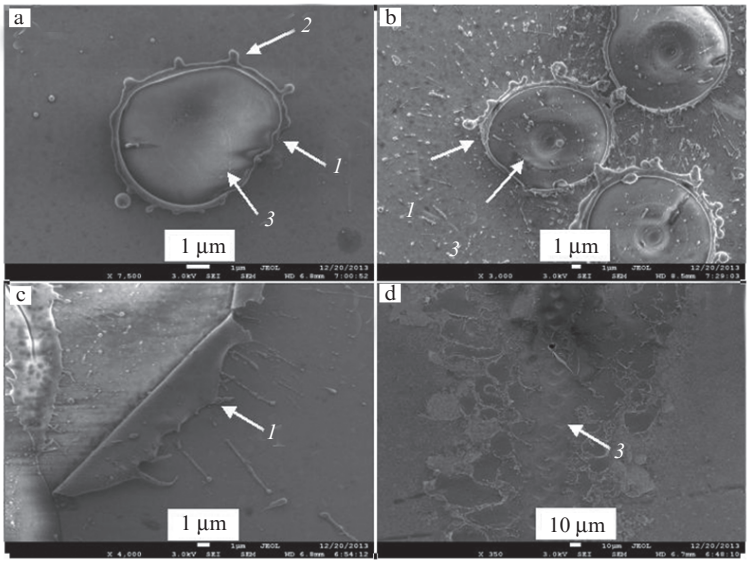

Figure 3. SEM photographs of microholes in the silver film with a thickness of 30 nm at nanosecond laser pulse energies E = (a) 9, (b) 47, (c) 180 and (d) 530 μJ: (*1*) hole edges; (*2*) 'frozen' nanojets; (*3*) internal craters on the glass substrate.

that, after focusing nanosecond laser radiation on the surface of thermally thin silver and chromium films with a release of high volumetric energy density in the focal region, the modification of the glass substrate only occurs in the focal region due to the low thermal conductivity of the glass, whereas the lateral energy transfer by means of electron thermal conductivity occurs in the metal film itself. Indeed, with regard to the known value of the thermal conductivity for silver $\chi_{Ag}(1000\ K) \approx 1.6\ cm^2\ s^{-1}$ [32], the characteristic size of the heat spot $R_{th}(\tau_{las}/2) \approx \sqrt{4\chi_{Ag}(\tau_{las}/2)}$ can reach 5 μm at the 1/e level in the middle of the laser pulse with a duration of $\tau_{las} \approx$ 75 ns, which is in good agreement with the observed values $w_{dep\,I}$ of about 2–4 μm. In the case of the chromium film, the twice smaller radius at comparable times of hole formation is associated with a substantially lower coefficient of thermal conductivity for chromium, which is in reasonable agreement with its known tabulated value $\chi_{Cr}(1000\ K) \leqslant 0.2\ cm^2\ s^{-1}$ [32].

Further, according to the estimates of the volumetric density of the input energy

$$\varepsilon(\Phi,h) \approx \frac{[1 - r(h) - t(h)]\,\Phi}{h},$$

where $r(h)$ and $t(h)$ are the reflectance and transmittance of a film with the thickness h at the heating wavelength of laser radiation, the characteristic values of ε for the threshold values $\Phi_{dep\,I}(h) = E_{dep\,I}/(\pi w^2_{dep\,I})$ correspond to the transformation of the film material into vapour by heating, melting and boiling with the total enthalpy $\Delta H^{vap}_{Ag} \approx 31\ kJ\ cm^{-3}$ and $\Delta H^{vap}_{Cr} \approx 59\ kJ\ cm^{-3}$ [32]. In the case of normal incidence, the coefficients $r(h) \approx 0.98$ and $t(h) \approx 0$ for silver films and $r(h) \approx 0.63$ and $t(h) \approx 0$ for chromium films were evaluated with regard to the tabulated optical constants for solids $n(1033\ nm) \approx 0.226$, $k(1033\ nm) \approx 6.99$ and $n(1069\ nm) \approx 4.53$, $k(1069\ nm) \approx 4.30$, respectively [33]. The evaporation phenomenon has previously been considered as the mechanism of the nanohole formation [5]; however, in the general case, the evaporation of homogeneously heated thin films is possible not only on the outer surface, but also at the film–substrate interface [34]. In the latter case, the vapour pressure in the emerging vapour cavity increases monotonically up to an equilibrium value, and at a certain threshold of the vapour pressure the film comes off. Some signs of this ablation (spallation) mechanism of the nanohole formation can be traced at the edge of the hole in the form of 'frozen' nanojets (Fig. 3a) or the traces of spatter on the periphery of the edge (Fig. 3b). With this evaporative mechanism of the film removal, the evaporation rate maximum is reached, (excluding the nonlinear thermal effects), exactly at the maximum of the emission intensity (in the middle of the laser pulse with a Gaussian time profile); however, the threshold pressure, as an integrated value, arises at the minimum value of Φ towards the end of the pulse. The threshold pressure differs considerably for different h, and in view of the decisive role of cohesion (the ablation occurs along the melt film and not at the film–substrate interface), the threshold pressure for thermally thin films nonlinearly increases with increasing thickness. This is due to the fact that, at comparable film thicknesses, we not only need to provide the comparable values of $\varepsilon \leqslant \Delta H^{vap}$ throughout the film depth (effect size), but also greater threshold pressures that are required to break the thicker films. This trend is indeed observed for silver films, for which not only the film ablation thresholds $\Phi_I(h)$, but also the characteristic radii of the holes (heat spot) $w_{dep\,I}$ increase monotonically with increasing h (2.5, 2 and 4 μm for the film of 30, 60 and 80 nm in thickness), which is indicative of a greater delay in their development, and hence of a larger radius of the heat spread due to the lateral heat conductivity. Furthermore, at a large film thickness and a relatively slow stage of removal (especially near the ablation threshold Φ_I), the films may be heated by the quantity ΔH^{vap} and completely vaporised even before the spallation, and not at the expansion stage.

Similarly, in the second regime, the characteristic radius of the crater on the glass surface is $w_{crat\,II} \approx 2$ μm for all types of the films (Table 1), which can be associated with the emerging erosive laser plasma, the area size of which increases monotonically according to the Gaussian distribution of the energy density at the focus when the breakdown threshold of the ablation products in the laser plume has been exceeded (the lower threshold for regime II is $\Phi_{crat\,II} = E_{crat\,II}/(\pi w^2_{crat\,II}) \sim 1–10\ kJ\ cm^{-2}$). The corresponding laser intensities of 30–80 GW cm^{-2} are inherent in the direct breakdown of the silicate glass [35–38]. This is quite possible with the rapid evaporation of the film at the forefront of a long laser pulse, which dramatically increases the threshold of vapour breakdown of the film material [39] and virtually eliminates it. Then the jump in the characteristic radius $w_{dep\,II}$ to 20–30 μm (up to ten times compared to $w_{dep\,I}$) can be associated with a longer heating of the film by bremsstrahlung and recombination radiation of plasma [40, 41]. Indeed, the estimates of the film heating time for $w_{dep\,II} \approx \sqrt{4\chi\tau^*}$, with regard to $\chi_{Ag}(1000\ K) \approx 1.6\ cm^2\ s^{-1}$ and $\chi_{Cr}(1000\ K) \leqslant 0.2\ cm^2\ s^{-1}$ [32], yield close values: $\tau^* \sim 1$ μs, and, according to a monotonically increasing dependence $w_{dep\,II}(h_{Ag})$, thicker films with larger $w_{dep\,II}$ again require longer heating for the formation of the higher vapour pressure of the vapour cavity in the vapour subsurface. Furthermore, since the energy input $\varepsilon_{II} \approx 5–13\ kJ\ cm^{-3}$ for the silver films is much less than the ΔH^{vap}, but larger than the corresponding value of the melt enthalpy $\Delta H^{melt} \approx 3.5\ kJ\ cm^{-3}$ [32], the occurrence of riving lateral expansion of the vapour cavity to the film periphery may be assumed, with removal of the film virtually along the boundary of the melt, which represents a quite unusual nonlocal mechanism of its ablation. In contrast, the abnormally high energy input $\varepsilon_{II} \approx 2\ MJ\ cm^{-3}$ at $\Phi_{dep\,II} \approx 21\ J\ cm^{-2}$ for chromium films indicates that the threshold energy $E_{dep\,II} \approx 33$ μJ, comparable with similar values for silver films (18–47 μJ) under similar conditions of focusing, represents a threshold for the plasma ignition, but not for the heating of these films.

Finally, the shock wave (SW) generated in the erosive plasma under the action of high-intensity laser radiation and well audible in the air (the threshold for regime III – $\Phi_{dep\,III} > 10\ kJ\ cm^{-2}$, the peak intensity $I_{las} \sim 10^2$ GW cm^{-2} for silver and chromium films) is capable of removing a thin silver film by the 'cold way', with characteristic size of the hole in regime III being almost 10 times greater than in regime II (Table 1), so that the volumetric density of the input energy at the edge of the area of the film removal does not even reach the melt enthalpy ΔH^{melt}. The edge of the hole has a wrapped outside film (Fig. 3d), the removal of which apparently can be associated with the shock-wave loading and subsequent removal of the film at the unloading stage by the hydrodynamic pressure of the ablation products from the central region of laser action. The estimates of the pressure p_{plas} and the temperature T_{plas} in the plasma core for these exposure conditions ($\lambda_{las} \approx 1064$ nm, $\tau_{las} \approx 75$ ns, $I_{las} \sim 10^2\ GW\ cm^{-2}$, silver with a molar mass A = 107, average ion charge number $Z = 4–5$) with the use of the expression [42]

$$p_{\text{plas}} = 5.83A^{-1/8}\Psi^{9/16}I_{\text{las}}^{3/4}(\lambda_{\text{las}}\sqrt{\tau_{\text{las}}})^{-1/4},$$
$$T_{\text{plas}} = 2.98\times10^{4}A^{1/8}(Z+1)^{-5/8}Z^{3/4}(I_{\text{las}}\lambda_{\text{las}}\sqrt{\tau_{\text{las}}})^{1/2}, \quad (1)$$

yield $p_{\text{plas}} \sim 10$ TPa and $T_{\text{plas}} \sim 200$ eV, where the factor $\Psi = 0.5A[Z^2(Z+1)]^{1/3}$. These values are quite sufficient for the spall of the film under the action of the air shock wave, although the latter may also excite a powerful surface acoustic wave to remove the film in shear mode.

It is noteworthy that until now the generally accepted technique for determining the parameters of the laser radiation focusing and energy density threshold during the surface modification is based on the use of the dependence of R^2 on $\ln(E/E_0)$ for estimating the characteristic radius of the modification area [43]. Obviously, this is true for the focusing conditions of several micrometers, when possible nonlocal nano- and micro-scale effects, such as blurring of the focal spot due to the thermal conductivity during the pump pulse [20], spread of the powerful shock waves from the focal volume, which modify the substance [44], as well as the observed effects of lateral heat conduction and the shock-wave effects, do not appear. Meanwhile, the results of this paper suggest that the physical picture near the thresholds of modifications can be much more complicated.

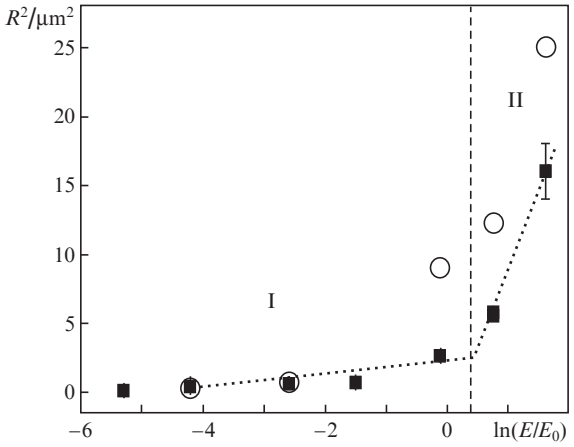

Figure 5. Dependences of the square of the radius R of holes in silver films with a thickness of 30 (○) and 60 nm (■) on the natural logarithm of the energy E/E_0 of femtosecond laser pulses for two regimes of laser action (I, II), with the corresponding characteristic radii $w_{\text{dep I}}(60\text{ nm}) = 0.7 \pm 0.2$ μm and $w_{\text{dep II}}(60\text{ nm}) = 3.0 \pm 0.5$ μm. The error in determining the square of the radius for the majority of the experimental points does not exceed the symbols size.

4. Formation of microholes by femtosecond laser radiation

When forming microholes in silver films by femtosecond laser radiation using a aspheric lens with the numerical aperture NA = 0.5, two different regimes are also observed (Figs 4, 5). In the first regime (I), wherein the apertures in the film have the diameters of 1–3 μm, the characteristic radii of apertures $w_{\text{dep I}}$ comprise 0.55 ± 0.2 μm (h = 30 nm) and 0.7 ± 0.2 μm (h = 60 nm) (Fig. 5), which significantly exceed the estimated radius of the focal spot $w_{\text{opt}}(515\text{ nm}) \approx 0.2$ μm for NA = 0.5. This discrepancy may be associated both with the errors of tight focusing (a slightly off-axis focus should lead to the formation of the holes ellipticity, which is not observed) and the lateral thermal conductivity in the films during the hole formation. It is noteworthy that the lower estimate of this time, carried out for a known value $\chi_{\text{Ag}}(1000\text{ K}) \approx 1.6\text{ cm}^2\text{ s}^{-1}$ [32], gives ~1 ns, which is quite consistent with the characteristic time of the electron–phonon relaxation of material ~10 ps (for the constant of the electron–phonon interaction $\sim10^{11}\text{ W cm}^{-3}\text{ K}^{-1}$ [45]) and the time of boiling onset ~1–10 ns [46] (see also related nanosecond dynamics of nanostructures formation – nanospikes and nanoedges – on the surface of metal films by means of femtosecond laser pulses [47]). This casts doubt on the advantage of using femtosecond laser pulses in the formation of the smallest possible nano- and microholes in the framework of the given evaporation mecha-

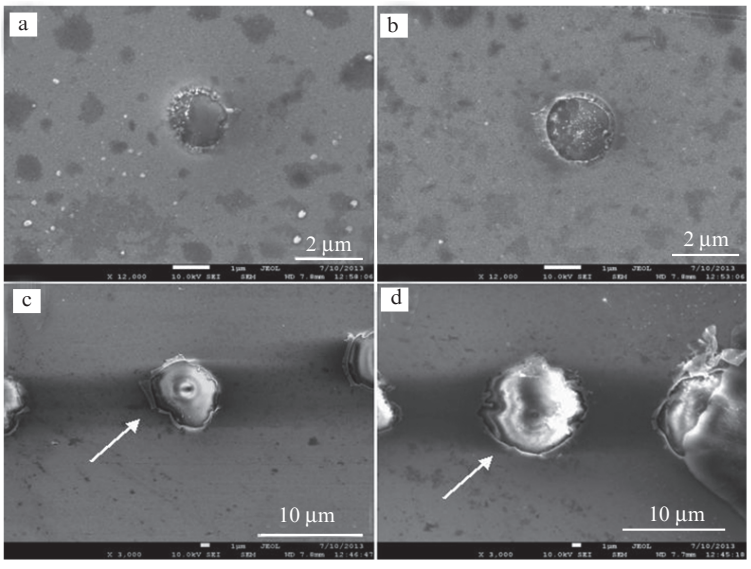

Figure 4. SEM photographs of microholes (shown by arrows) in the silver film with a thickness of 30 nm at femtosecond laser pulse energies E = (a) 15 and (b) 75 nJ as well as at (c) 2.2 and (d) 5 μJ.

nism as compared, for example, with the sub-nanosecond and picosecond laser pulses. Herewith, the threshold values of Φ_{I} amount to 0.6 ± 0.2 J cm^{-2} (h = 30 nm) and 1.0 ± 0.3 J cm^{-2} (h = 60 nm), which, with regard to the reflection coefficient of the unexcited silver surface at the normal incidence R(515 nm) ≈ 0.75 for n(516.6 nm) ≈ 1.9 and k(516.6 nm) ≈ 4.7 [33], really meets the volumetric density of the input energy $\varepsilon_{\mathrm{I}} \approx 40-50$ kJ cm^{-3} at the enthalpy of vapour $\Delta H^{\mathrm{vap}} \approx 32$ kJ cm^{-3} [32].

In the regime of more intense femtosecond laser irradiation with the same focusing (see the craters of submicron and micron size on the glass substrate inside the holes in the film in Fig. 4d) but with a higher threshold energy (more than 1 μJ), the microholes are subjected to some changes, i.e., their diameter increases to about 5 μm (Fig. 5) and the right circular form which is inherent for the low energies (Figs 4a and 4b) turns out significantly distorted (Figs 4c and 4d). In this case, the calculated laser fluence Φ reaches 50–100 J cm^{-2}, which corresponds to the peak intensity of $\sim(1-2)\times 10^2$ TW cm^{-2}. In fact, even at lower intensities, due to the interference between the incident and reflected femtosecond laser radiation, a near-surface air plasma column occurs [48], causing radiation defocusing [49]. The ablative removal of the film from the region with a characteristic radius $w_{\mathrm{dep\,II}} \approx 2-3$ μm can be either carried out directly by a partially defocused pulse with participation of the lateral thermal conductivity, or under the influence of plasma heating or shock-wave effects [48] (see the torn edges of the film along the edges of the hole in Fig. 4c). More precisely, the estimate of the volumetric density of the input energy $\varepsilon \approx (1-R)\Phi_{\mathrm{II}}/h \sim 10^2$ kJ cm^{-3} at normal incidence for $\Phi_{\mathrm{II}} = E_{\mathrm{II}}/(\pi w^2_{\mathrm{dep\,II}}) \approx 3-6$ J cm^{-2}, which is self-consistent with regard to $w_{\mathrm{dep\,II}}$ on plasma defocusing (but not absorption in the plasma, which, however, is small [48–50], and the difficult-to-predict average reflectance of the photoexcited film), indicates a high probability of thermal nature of the film removal.

Thus, the nonlocal ablative effects associated with the nanosecond lateral heat conductivity and long-term heating of the film through the bremsstrahlung from plasma (or even its shock-wave action) manifest themselves in the formation of holes in thin films even with ultrashort (in this case, femtosecond) laser pulses.

5. Conclusions

We have considered the mechanisms of formation of the submicron- and microscale holes in thin silver and chrome films on the glass substrates under the action of the single femtosecond and nanosecond laser pulses, tightly focused in the focal spot diameter of ~ 1 μm. It is shown that the holes with a minimum diameter are formed at small (1–100 nJ) energies of these pulses in accordance with the evaporation mechanism, preceded by the nanosecond lateral thermal conductivity in the films. This essentially negates the advantage of the duration of the laser exposure by ultrashort laser pulses. At a higher (more than 1 μJ) energy of femtosecond laser pulses, large-scale ablative effects associated with the defocusing of radiation in the air plasma and plasma heating or shock-wave action appear. Similarly, for nanosecond laser pulses with the energies less than 1 mJ, the plasma heating and evaporation of the film or even its removal from the erosive plasma by the action of the air shock-wave is observed. In all cases, the nonlocal effects of the laser exposure take place, manifesting themselves in the lateral heat conduction during the formation of holes, the riving lateral expansion of the sub-surface vapour cavity or in the long-term plasma shock-wave action.

Acknowledgements. This work was partially supported by the Russian Foundation for Basic Research (Grant No. 13-02-00971-a) and the Presidium of RAS (Fundamentals of Technology of Nanostructures and Nanomaterials and Extreme Light Fields and Their Applications Programmes).

References

1. Genet C., Ebbesen T.W. *Nature*, **445**, 39 (2007).
2. Melentiev P.N., Konstantinova T.V., Afanasiev A.E., Kuzin A.A., Baturin A.S., Balykin V.I. *Opt. Express*, **20**, 19474 (2012).
3. Koch J., Korte F., Bauer T., Fallnich C., Ostendorf A., Chichkov B.N. *Appl. Phys. A*, **81**, 325 (2005).
4. Nakata Y., Okada T., Maeda M. *Jpn. J. Appl. Phys*., **42**, L1452 (2003).
5. Nakata Y., Miyanaga N., Okada T. *Appl. Surf. Sci*., **253**, 6555 (2007).
6. Moening J.P., Georgiev D.G. *J. Appl. Phys*., **107**, 014307 (2010).
7. Moening J.P., Thanawala S.S., Georgiev D.G. *Appl. Phys. A*, **95**, 635 (2009).
8. Willis D.A., Grosu V. *Appl. Phys. Lett*., **86**, 244103 (2005).
9. Banks D.P., Grivas C., Mills J.D., Eason R.W., Zergioti I. *Appl. Phys. Lett*., **89**, 193107 (2006).
10. Kuznetsov A.I., Koch J., Chichkov B.N. *Opt. Express*, **17**, 18820 (2009).
11. Sinton D., Gordon R., Brolo A.G. *Microfluid. Nanofluid*, **4**, 107 (2008).
12. Kuznetsov A.I., Evlyukhin A.B., Goncalves M.R., Reinhardt C., Koroleva A., Arnedillo M., Kiyan R., Marti O., Chichkov B.N. *ASC Nano*, **5**, 4843 (2011).
13. Gordon R., Brolo A.G., Sinton D., Kavanagh K. *Laser Photonics Rev*., **4**, 311 (2010).
14. Neubrech F., Pucci A., Cornelius T.W., Karim S., Garcia-Etxarri A., Aizpurua J. *Phys. Rev. Lett*., **101**, 157403 (2008).
15. Pronko P.P., Dutta S.K., Squier J., Rudd J.V., Du D., et al. *Opt. Commun*., **114**, 106 (1995).
16. Korte F., Serbin J., Koch J., Egbert A., Fallnich C., Ostendorf A., Chichkov B.N. *Appl. Phys. A*, **77**, 229 (2003).
17. Kuznetsov A.I., Koch J., Chichkov B.N. *Appl. Phys. A*, **94**, 221 (2009).
18. Kuznetsov A.I., Unger C., Koch J., Chichkov B.N. *Appl. Phys. A*, **106**, 479 (2012).
19. Guo Z., Feng J., Zhou K., Xiao Y., Qu S., Lee J.-H. *Appl. Phys. A*, **108**, 639 (2012).
20. Kulchin Yu.N., Vitrik O.B., Kuchmizhak A.A., Nepomnyashchii A.V., Savchuk A.G., Ionin A.A., Kudryashov S.I., Makarov S.V. *Opt. Lett*., **38**, 1452 (2013).
21. Moening J.P., Georgiev D.G., Lawrence J.G. *J. Appl. Phys*., **109**, 014304 (2011).
22. Chong T.C., Hong M.H., Shi L.P. *Laser Photonics Rev*., **4**, 123 (2010).
23. Chichkov B.N., Momma C., Nolte S., Alvensleben F.V., Tünnermann A. *Appl. Phys. A*, **63**, 109 (1996).
24. Koch J., Korte F., Fallnich C., Chichkov B.N. *Opt. Eng*., **5**, 051103 (2005).
25. Kuznetsov A.I., Koch J., Chichkov B.N. *Appl. Phys. A*, **94**, 221 (2008).
26. Meshcheryakov Y.P., Bulgakova N.M. *Appl. Phys. A*, **82**, 363 (2005); Meshcheryakov Y.P., Shugaev M.V., Mattle Th., Lippert Th., Bulgakova N.M. *Appl. Phys. A*, **113** (2), 521 (2013).
27. Ivanov D.S., Rethfeld B.C., O'Connor G.M., et al. *Appl. Phys. A*, **92**, 791 (2008).
28. Ionin A.A., Kudryashov S.I., Seleznev L.V., et al. *Zh. Eksp. Teor. Fiz*., **143**, 403 (2013).
29. Lee S.K., Chang W.S., Na S.J. *J. Appl. Phys*., **86**, 4282 (1999).
30. Vrij A. *Discuss. Faraday Soc*., **42**, 23 (1966).
31. Bischof J., Scherer D., Herminghaus S., Leiderer P. *Phys. Rev. Lett*., **77**, 1536 (1996).

32. Grigoriev I.S., Meilikhov E.Z. (Eds.) *Handbook of Physical Quantities* (Boca Raton, FL: CRC Press, 1997; Moscow: Energoatomizdat, 1991).
33. Palik E.D. (Ed.) *Handbook of Optical Constants of Solids* (Orlando: Academic Press, 1998).
34. Kudryashov S.I., Allen S.D. *J. Appl. Phys*., **95**, 5820 (2004); Kudryashov S.I., Allen S.D. *Appl. Phys. A*, **79**, 1737 (2004).
35. Du D., Lui X., Korn G., Squier J., Mourou G. *Appl. Phys. Lett*., **64**, 3071 (1994).
36. Stuart B.C., Feit M.D., Herman S., Rubenchik A.M., Shore B.W., Perry M.D. *Phys. Rev. B*, **53**, 1749 (1996).
37. Smith A.V., Do B.T. *Appl. Opt*., **47**, 4812 (2008).
38. Cahoon E.M., Amirall J.R. *Appl. Opt.*, **49**, C49 (2010).
39. Ionin A.A., Kudryashov S.I., Seleznev L.V. *Phys. Rev. E*, **82**, 016404 (2010).
40. Paul S., Kudryashov S.I., Lyon K., Allen S.D. *J. Appl. Phys*., **101**, 043106 (2007).
41. Bulgakova N.M., Evtushenko A.B., Shukhov Yu.G., Kudryashov S.I., Bulgakov A.V. *Appl. Surf. Sci*., **257**, 10876 (2011).
42. Phipps C.R., Turner T.P., Harrison R.F., York G.W., Osborne W.Z., Anderson G.K., Corlis X.F., Haynes L.C., Steele H.S., Spicochi K.C., King T.R. *J. Appl. Phys*., **64**, 1083 (1988).
43. Liu J.M. *Opt. Lett*., **7**, 196 (1982).
44. Gamaly E., Juodkazis S., Nishimura K., Misawa H., Luther-Davies B., Hallo L., Nicolai P., Tikhonchuk V. *Phys. Rev. B*, **73**, 214101 (2006).
45. Lin Z., Zhigilei L.V., Celli V. *Phys. Rev. B*, **77**, 075133 (2008).
46. Lindenberg A.M., Engemann S., Gaffney K., Sokolowski-Tinten K., Larsson J., Hillyard P.B., Reis D.A., Fritz D.M., Arthur J., Akre R.A., George M.J., Deb A., Bucksbaum P.H., Hajdu J., Meyer D.A., Nicoul M., Blome C., Tschentscher Th., Cavalieri A.L., Falcone R.W., Lee S.H., Pahl R., Rudati J., Fuoss P.H., Nelson A.J., Krejcik P., Siddons D.P., Lorazo P., Hastings J.B. *Phys. Rev. Lett*., **100**, 135502 (2008).
47. Unger C., Koch J., Overmeyer L., Chichkov B.N. *Opt. Express*, **20**, 24864 (2012).
48. Bulgakova N.M., Zhukov V.P., Vorobyev A.Y., Guo C. *Appl. Phys. A*, **92**, 883 (2008).
49. Klimentov S.M., Kononenko T.V., Pivovarov P.A., Konov V.I., Prokhorov A.M., Breitling D., Dausinger F. *Kvantovaya Elektron*., **32**, 433 (2002) [*Quantum Electron*., **32**, 433 (2002)].
50. Ionin A.A., Kudryashov S.I., Makarov S.V., Seleznev L.V., Sinitsyn D.V. *Pis'ma Zh. Eksp. Teor. Fiz*., **90** (6), 471 (2009).